AIAA JOURNAL
Vol. 32, No. 7, July 1994

Technical Notes

TECHNICAL NOTES are short manuscripts describing new developments or important results of a preliminary nature. These Notes cannot exceed 6 manuscript pages and 3 figures; a page of text may be substituted for a figure and vice versa. After informal review by the editors, they may be published within a few months of the date of receipt. Style requirements are the same as for regular contributions (see inside back cover).

Lift Analysis of a Variable Camber Foil Using the Discrete Vortex-Blob Method

B. J. Maclean* and R. A. Decker†
University of Utah, Salt Lake City, Utah 84112

Introduction

RECENT research activities in the area of active or "smart" material systems have generated significant interest to develop adaptive lifting surfaces for advanced aircraft and submarine structures. By using integrated actuators and sensors, advanced problems are being addressed in aeroelastic tailoring, vibration and attitude control, and high lift devices.[1–6] For example, on submarine aftbodies, compliant attitude control appendages that utilize large out-of-plane foil deformation can provide enhanced lift with reduced wake disturbance compared to conventional full-flying and trailing-edge flapped designs.[7–9] To quantify the performance improvements of such control surfaces, an analysis technique is required which can model separated flow at high Reynolds numbers and provide pressure distributions for structure and control system design. The purpose of this Note is to present use of a discrete vortex-blob method to compare lift performance between fixed and variable camber NACA 0012 foils at a Reynolds number of 1×10^7 for incompressible flow in two dimensions. The vortex method provides a natural and numerically efficient description of eddies and the vorticity they carry. Since a large number of discrete vortex blobs are used to produce a vorticity field in a Lagrangian reference frame, the method becomes grid free and allows modeling of unsteady flows[10] even around multielement bodies of arbitrary shape (conformal mappings are not involved) in nonuniform motion or rotation.

Formulation of the Discrete Vortex-Blob Method

The discrete vortex-blob method, furthered by Spalart and coworkers[11,12] at NASA Ames Research Center, and incorporated in the computer code KPD12, is based on a vorticity formulation of the Navier-Stokes equations for incompressible flow in two dimensions:

$$\frac{\partial \omega}{\partial t} + u\frac{\partial \omega}{\partial x} + v\frac{\partial \omega}{\partial y} = \nu\left(\frac{\partial^2 \omega}{\partial x^2} + \frac{\partial^2 \omega}{\partial y^2}\right) \tag{1}$$

where ω is the scalar quantity of vorticity (equal to two times the local angular velocity) with u and v velocity components in the x and y directions, respectively, over time t, and ν is the kinematic viscosity. The incompressibility is implicit and the pressure term has dropped out, leaving one equation with one unknown since a velocity field (if the fluid is incompressible) can be obtained from a vorticity field by using the Biot-Savart law. The boundary conditions are as follows:

1) At the boundary of a solid, the velocity of the fluid equals the velocity of the solid; this is the application of the no-slip condition which results in the Kutta condition for developing flows which are initially irrotational.

2) Flow tends toward the freestream velocity U_∞ at large distances from the body.

3) The initial conditions for U at time equals zero are considered given.

4) There is no initial circulation. No boundary conditions are needed for the pressure.

The flow can be treated as inviscid away from the solid walls since large features dominate in the wake and are not very sensitive to viscosity. This reduces Eq. (1) to an inviscid transport equation for vorticity and is ideally suited to a Lagrangian description because vorticity is conserved over time. Compared with finite difference methods using an Eulerian formulation, the vortex-blob method presents no obvious numerical dispersion, allowing large time steps to be taken within acceptable limits for accuracy. Moreover, it requires much less computer memory since all flowfield information is carried by the discrete vortices which are concentrated in areas of high gradients. Thus, the problem is first discretized by establishing a large number of mobile vortices which are transported through the domain. The vorticity field is then defined by summing the contribution of each vortex

$$\omega(\boldsymbol{r}) = \sum_{i=1}^{N_v} \Gamma_i \gamma(|\boldsymbol{r} - \boldsymbol{r}_i|) \tag{2}$$

where N_v is the total number of vortices, $\boldsymbol{r}_i$ is the center position of the ith blob, Γ_i is the circulation of the ith blob, and γ is the strength profile or core function (generally bell-shaped, contributing the word blob to the name for the method). Similarly, vorticity and stream function follow Poisson's equation, allowing determination of solid surface boundaries by adjusting the strength of new vortices as they are introduced into the flowfield near the solid body. Two additional equations are required to close the system, namely, that each blob retains its circulation in time so that total vorticity is conserved and each vortex follows the flow like a particle.

$$\frac{\mathrm{d}\Gamma_i}{\mathrm{d}t} = 0 \tag{3}$$

$$\frac{\mathrm{d}\boldsymbol{r}_i}{\mathrm{d}t} = \boldsymbol{U}(\boldsymbol{r}_i, t) \tag{4}$$

The velocity components attributed to the vorticity field at point $\boldsymbol{r}$ are calculated using the Biot-Savart law:

$$\begin{bmatrix} u \\ v \end{bmatrix}(\boldsymbol{r}) = \sum_{i=1}^{N_v} \frac{\Gamma_i}{2\pi} \eta(|\boldsymbol{r} - \boldsymbol{r}_i|) \begin{bmatrix} y_i - y \\ x - x_i \end{bmatrix} \tag{5}$$

where η is defined by

$$\frac{\mathrm{d}(r^2\eta)}{\mathrm{d}r} = r\gamma(r) \text{ and } \eta \approx r^{-2} \text{ for } r \text{ large} \tag{6}$$

Received Aug. 13, 1993; revision received Jan. 5, 1994; accepted for publication Jan. 14, 1994.

*Graduate Student; currently at Sarcos Research Corporation, Salt Lake City, Utah. Member AIAA.

†Assistant Professor, Department of Civil Engineering, Computational Fluid Dynamics Laboratory. Member AIAA.

Equation (6) is greatly simplified by the fact that the blobs are axisymmetric and provide a smooth function across their centers (for a point vortex, $\eta = r^{-2}$ which is singular at its center). The surface pressure distribution can be accurately determined at any time using the incompressible Bernoulli's equation in regions which are irrotational (e.g., from the stagnation point of an airfoil along its surface to the point of separation) and using the wall vorticity relation in regions which are rotational

$$\frac{DU}{Dt} \cdot t = -\frac{1}{\rho}\frac{\partial P}{\partial s} + \nu \frac{\partial \omega}{\partial n} \tag{7}$$

where t is the unit vector tangent to the airfoil surface, U is the velocity vector, P is the pressure, ρ is the density, and s and n are the streamwise and normal component directions of the foil surface, respectively.

The premature separation of vortices on airfoil geometries is artifically prevented in KPD2 on the basis of boundary-layer calculations using simple integral methods (Thwaites' method for the laminar part, Head's method for the turbulent part, and Schlichting-Granville for transition). The numerical implementation proceeds for each time step as follows. 1) Determine the pressure distribution around the foil using Eq. (7) and the velocities calculated from Eq. (5). 2) Use pressure as a forcing function to solve the boundary-layer equations from the stagnation point to the first separation point (Bernoulli's theorem applies in this region upstream of separation). 3) Create a layer of temporary vortices upstream of the desired separation point and a layer of permanent vortices downstream of the separation point along the surface of the solid body (the boundary condition is satisfied by solving a system of linear equations to determine the strengths of new vortices at each time step and, thereby, force a constant stream function value along the body's surface; the strengths of these vortices are then preserved during transport). 4) Advance the vortices in time using the second-order Adams-Bashforth scheme to minimize scattering (the explicit Euler scheme is used for the first multiple point). 5) Merge permanent vortices which are transported far downstream to maintain a relatively constant total number of vortices (to prevent growth of computer memory requirements). 6) Delete the temporary vortices and any vortices that hit a wall. 7) Solve the vorticity field using Eq. (2). Finally, 8) return to step 1.

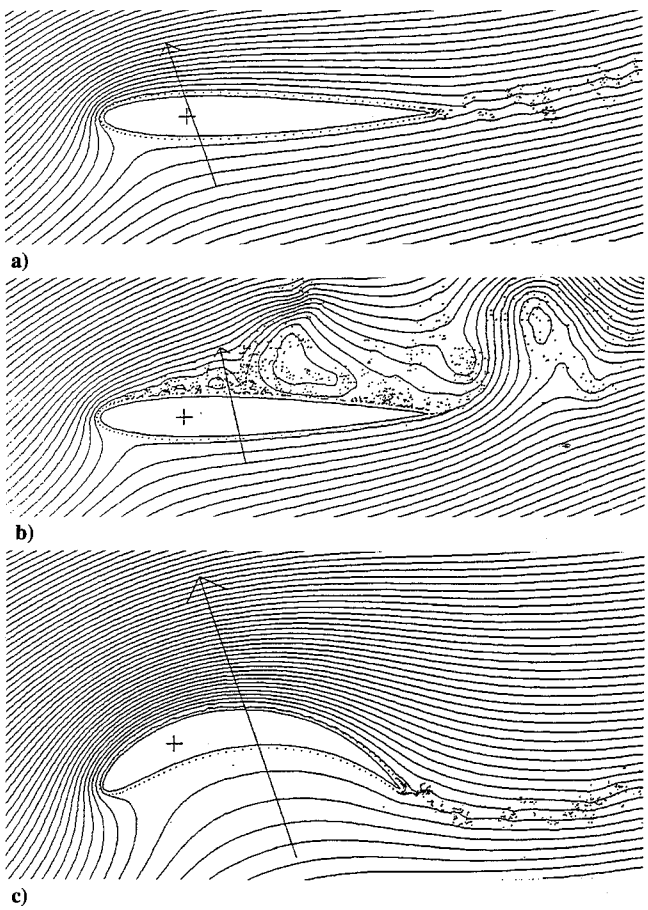

Fig. 1 Flowfield comparison for rigid and compliant NACA 0012 airfoil sections at $Re = 1 \times 10^7$ (contour lines are streamlines): a) 20-deg AOA, b) 25-deg AOA, and c) 25-deg AOA.

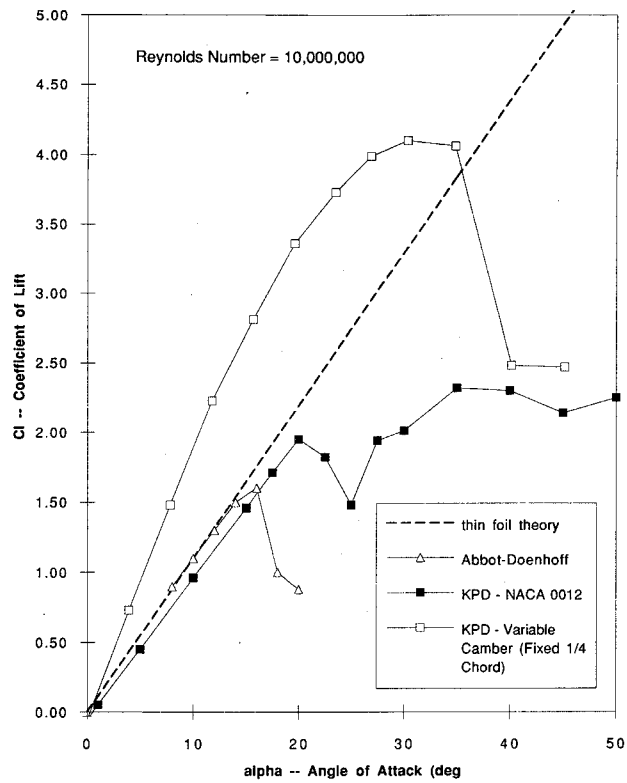

Fig. 2 Analytic comparison of lift performance for rigid and compliant NACA 0012 airfoils.

Analysis Results for Compliant vs Rigid NACA 0012 Foils

A copy of the KPD12 code, vectorized for a Cray Y-MP, was modified to be compatible with the Fortran compiler on a Silicon Graphics IRIS-Indigo workstation. Preliminary analysis of a NACA 0012 foil was conducted at $Re = 1 \times 10^7$ to establish acceptable input parameters without making execution time excessive. Since modeling begins from a dead startup, i.e., there is no net circulation around the solid body until the startup vortex is shed downstream, adequate time is needed to effectively time average the unsteady nature of the flow as well as mask the startup transients. Using 100 body coordinates with 1600 vortices for 1000 nondimensional time steps of 0.01 provided an effective balance between fidelity of results and execution time (between 2.5 and 3.0 h per run). Body coordinates were also generated for the same NACA 0012 foil but for a variety of different cambers, each with constant curvature. The coordinates were then rotated to establish a fixed quarter-chord location with zero tangential incidence relative to the uniform freestream. This provided the basis for a series of computer runs to directly compare the performance of a rigid foil gimbaled about its quarter chord with a compliant foil which is fixed at quarter chord and accomplishes lift through out-of-plane deformation fore and aft of this location.

Figures 1a and 1b graphically shows the transition of the rigid foil from attached flow at 20 deg to fully separated flow at 25-deg angle of attack (AOA). Also shown are the discrete vortex-blob creation points around the body and their transport into the body's wake. For 20-deg AOA at this Reynolds number the flow transitions early, promoting adherence, and the force vector indicates a classical location for center of pressure near the quarter chord. At

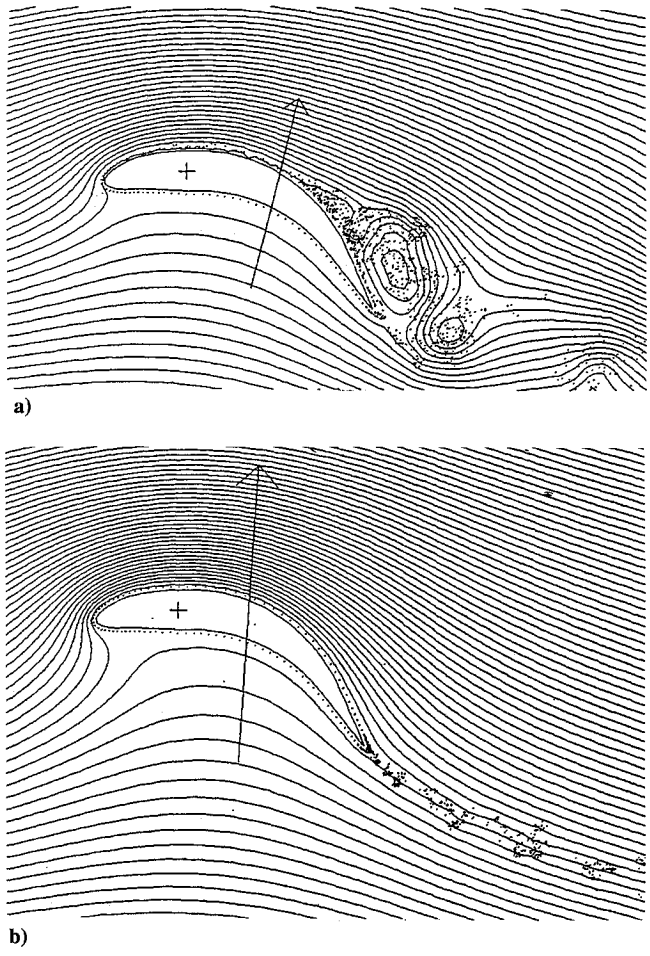

Fig. 3 Reynolds number dependence of separation over airfoil section at 25-deg AOA (contour lines are streamlines): a) $Re = 1 \times 10^6$ and b) $Re = 1 \times 10^7$.

25-degree AOA, the relative magnitude of the lift vector is diminished and pressure drag increases along with forward pitching moment, all a result of the separated flow and wake disturbance (the coefficient of moment is inferred by position and magnitude of the force vector relative to the quarter chord). Figure 1c shows the compliant foil with the same AOA of 25 deg, but with 21% constant curvature camber. The magnitude of lift is twice that of the rigid foil before stall, producing a calculated C_L of 3.73. The fact that center of pressure moves aft with increases in camber is clearly seen, but there is little or no pressure drag.

Of prime interest is the magnitude of additional lift possible with the compliant foil before it stalls. Figure 2 shows a comparison of lift vs AOA for the two foils at $Re = 10 \times 10^6$. The rigid foil closely follows the lift slope of 2π predicted by thin foil theory until approximately 20 deg (lift values are slightly less than theoretical due to time averaging of the startup transient when foil circulation is still developing). After reaching a maximum C_L of about 1.9, stall is precipitated until 30 deg, at which time an unreasonably organized separated flow region above the foil re-establishes lift by way of upstream flow. By comparison, the compliant foil continues building lift with its concurrent increases in camber and effective AOA to a maximum $C_L > 4.0$. Even though the KPD prediction for stall of the rigid NACA 0012 is approximately 4 deg higher than experimental data,[13] the analytic comparison still suggests a factor of two increase in maximum lift. By adjusting the empirical constants in the integral boundary-layer solvers, the KPD code can be used to match the experimental data for the rigid foil and, thereby, predict a more reasonable but respectable maximum C_L of about 3.2 (an Eppler code predicted a maximum C_L of 3.3 for this same foil geometry, angle of attack, and Reynolds number).

However, this performance may be diminished because not all chordwise portions of an actual test article would be available for actuation. As an example, a more realistic body geometry was generated restricting curvature changes to stations between 6 and 20% of chord and between 30 and 80% of chord. The "wing box" was fixed at zero incidence to the freestream and a uniform radius of curvature of 50% chord was applied to the active sections of the foil. This was presribed to produce the same 25-deg AOA relative to the freestream as the 21% camber foil shown earlier in Fig. 1c. Results of this run are shown in Fig. 3a where flow remains attached and a C_L of 3.74 was calculated. Apparently, sharper changes in curvature will be required at this Reynolds number to induce separation. To test the Reynolds number dependence of flow separation, the same foil was run at one-tenth the velocity ($Re = 1 \times 10^6$). Figure 3b shows the loss in lift and increase in pressure drag as separation begins. Even though both of these flows have transitioned on the upper surface, the KPD code has utilized the boundary-layer solvers to predict where, if any, separation should occur.

Future Work

In summary, the KPD code should serve as a viable analytic tool to compare two-dimensional performance of compliant foil configurations with full-flying rigid and trailing-edge flapped baseline designs for attitude control surfaces, as well as other configurations for advanced lifting surfaces. Calculated pressure distributions, for example, will be critical for determining applied load inputs to finite element modeling of actual test hardware. Future work on this project will include the design, fabrication, and wind-tunnel testing of the compliant NACA 0012 foil described earlier to validate the KPD2 analytic predictions presented in Fig. 2. Of particular interest will be the later coupling of KPD2 to an analytic structural model so that camber optimization algorithms can be evaluated based on discrete surface pressure calculations.

References

[1]Smith, F. R., Harshberger, G. W., and Ujcik, V. G., "AFTI/F-111 Performance Flight Test Summary," Society of Automotive Engineers Aerospace Technology Conf. and Expo., Long Beach, CA, Oct. 5–8, 1987.

[2]Redecker, G., Wichman, G., and Oelker, H., "Aerodynamic Investigations Toward an Adaptive Airfoil for a Transonic Transport Aircraft," *Journal of Aircraft*, Vol. 23, No. 5, 1986, pp. 398–405.

[3]Crawley, E. F., and Lazarus, K. B., "Induced Strain Actuation of Isotropic and Anisotropic Plates," *Proceedings of the AIAA/ASME/ASCE/AHS/ASC 30th Structures, Structural Dynamics, and Materials Conference* (Mobile, AL), AIAA, Washington, DC, 1989 (AIAA Paper 89-1326).

[4]Chopra, I., "Development of an Intelligent Rotor," *Active Materials and Adaptive Structures*, edited by G. J. Knowles, Institute of Physics Publishing, Philadelphia, PA, 1991, pp. 271–275.

[5]Crawley, E. F., Lazarus, K. B., and Bohlmann, J. D., "Static Aeroelastic Control Using Strain Actuated Adaptive Structures," *Journal of Intelligent Material Systems and Structures*, Vol. 2, July 1991, pp. 386–410.

[6]Ikegami, R., Wilson, D. G., and Laakso, J. H., "Active Vibration Control Using NiTiNOL and Piezoelectric Ceramics," *Journal of Intelligent Material Systems and Structures*, Vol. 1, April 1990, pp. 189–206.

[7]Beauchamp, C., Nadoling, R., and Dean, L., "Shape Memory Alloy Articulated (SMAART) Control Surfaces," *Proceedings of the Conference on Active Materials and Adaptive Structures*, edited by G. J. Knowles, Institute of Physics, Philadelphia, PA, 1991, pp. 455–460.

[8]Maclean, B. J., Carpenter, B. F., Draper, J. L., and Misra, M. S., "A Compliant Wing Section for Adaptive Control Surfaces." *Proceedings of the Conference on Active Materials and Adaptive Structures*, edited by G. J. Knowles, Institute of Physics, Philadelphia, PA, 1991, pp. 281–284.

[9]Maclean, B. J., Carpenter, B. F., Draper, J. L., and Misra, M. S., "A Shape Memory Actuated Compliant Control Surface," *Proceedings of SPIE/ASME/SEM 1993 North American Conference on Smart Structures and Materials*, SPIE Proceedings, Vol. 1917, International Society for Optical Engineering, Ballingham, WA, 1993, pp. 809–818.

[10]Laurie, K. B., and Farokhi, S., "Separated Flowfield and Lift on an Airfoil with an Oscillating Leading-Edge Flap," AIAA Paper 93-3422, Aug. 1993.

[11]Spalart, P. R., Leonard, A., and Baganoff, D., "Numerical Simulation of Separated Flows," NASA TM 84328, Feb. 1983.

[12]Spalart, P. R., "Vortex Methods for Separated Flows," NASA TM 100068, June 1988.

[13]Abbot, I. H., and Von Doenhoff, A. E., *Theory of Wing Sections*, Dover, New York, 1959, p. 462.